MRS Advances (2024) 9:803–809
https://doi.org/10.1557/s43580-024-00827-y

ORIGINAL PAPER

Enhanced photocatalytic and antibacterial performance of $NiCo_2S_4$ nanostructures

A. B. Shanmugapriya[1] · R. Mary Mathelane[1] · A. Juliet Christina Mary[1] · A. Jegatha Christy[1] · Suresh Sagadevan[2]

Received: 27 December 2023 / Accepted: 12 March 2024 / Published online: 3 April 2024

Abstract

In this study, $NiCo_2S_4$ nanostructures are synthesized to investigate their antibacterial and photocatalytic activities. Thiourea is used to control the growth rate of nanoparticles. The photocatalytic activity of the $NiCo_2S_4$ nanostructures are tested using the popular dye amaranth. Photodegradation of the amaranth dye resulted in a higher efficiency of the $NiCo_2S_4$ nanostructures. The nano-sized $NiCo_2S_4$ has enhanced the dye degradation efficiency owing to the dual effects of adsorption and photodegradation. Furthermore, the antibacterial activity of the $NiCo_2S_4$ nanostructures against different bacterial strains of *Escherichia coli*, *Pseudomonas aeruginosa*, *Staph aureus*, and *Bacillus subtilis* are determined by the Kirby-Bauer method. $NiCo_2S_4$ nanostructures have shown superior antibacterial activity against both Gram-positive and Gram-negative bacteria, with maximum inhibition zones of 20 and 18 mm, respectively.

Introduction

The development of nanotechnology has provided the world with a new potential global approach because of its applications in various fields. The special features of nanoparticles are widely used in various applications, especially in electronics, photocatalysis, energy reservoirs, medicine, cosmetics, biomedical devices, automobiles, packaging, antibacterial, and information technology [1–5]. Most of the transition metal oxide/sulfide nanosheets are transparent exhibiting an excellent electrical and thermal properties. Various metal oxide/sulfide nanoparticles, such as ZnO, TiO_2, CdO, CuO, $NiCo_2S_4$, and Fe_2S_4, have been synthesized for many applications because of their superior structural, optical, and biological properties [6–10]. $NiCo_2S_4$ with spinel structured material reveals high conductivity, rich in redox sites enables superior catalytic activity and outstanding bioactivity, and also enhances stability during redox processes. Owing to their superior electrocatalytic performance and long life, $NiCo_2S_4$ is widely used in photocatalytic and antimicrobial applications. $NiCo_2S_4$ is mostly synthesized by the hydrothermal method because this method has more beneficial for obtaining homogeneous particles with less agglomeration. Commercial textile dyes are mixed with wastewater at different concentrations. Dye pollutants are the main cause of aqueous environmental contamination; therefore, it must be removed from wastewater. Wastewater discharged from industries, utilize various types of synthetic dyes, which are extremely poisonous and carcinogenic, and hence, effectively treated with photocatalysis to oxidize several organic contaminants and remove colors. Tar, a dark red to purple azo dye that is primarily used to color cosmetics, has the source of an anionic dye known as amaranth dye [11–13]. It can be used to color phenol–formaldehyde resins, leather, paper, natural and synthetic fibers, etc. This study highlights the use of hydrothermally produced $NiCo_2S_4$ for the removal of amaranth dye in an aqueous solution. $NiCo_2S_4$ acts as an absorbent to adsorb dye molecules and photodegrade the dye, leading to an increase in dye removal efficiency.

Owing to their safety, nutritional value, health benefits, and antibacterial activity, antibiotics have recently attracted the attention of researchers. This motivated us to investigate the $NiCo_2S_4$ nanoparticles. $NiCo_2S_4$ exhibited dose-dependent antibiotic activity against both gram-negative and gram-positive bacteria. *Staphylococcus aureus* and *Bacillus* are the two common gram-positive bacteria employed in

✉ R. Mary Mathelane
marymathelanephy@annejac.ac.in

✉ Suresh Sagadevan
drsureshsagadevan@um.edu.my

[1] PG and Research Centre of Physics, Jayaraj Annapackiam College for Women (Autonomous), Periyakulam, Tamilnadu 625 601, India

[2] Nanotechnology & Catalysis Research Centre, University of Malaya, 50603 Kuala Lumpur, Malaysia

the processing of meat products. *Staphylococcus aureus* is a gram-positive foodborne pathogen that contaminates diverse foods worldwide. *E. coli*, a gram-negative bacterium, is used to detect fecal contamination in food. This may result in a number of side effects such as diarrhea and gastroenteritis. The antibacterial and antiviral activities of nanoparticles are associated with compounds that completely kill bacteria and viruses or slow down their growth rate [14–16].

In this study, $NiCo_2S_4$ (NCS) nanostructure was synthesized using a hydrothermal method, and the structural, morphological, antibacterial, and photocatalytic activities of the material are investigated. The superior nature of this material inspired us to study its catalytic and biological activities. Almost 93% of degrading efficiency are observed for the synthesized $NiCo_2S_4$ nanomaterial after 120 min of the degradation process, which proves the superior catalytic behavior of the material. Also, $NiCo_2S_4$ nanomaterial proved to be an effective antibacterial agent against both Gram-positive (*Staph aureus*, *Bacillus subtilis*) and Gram-negative (*Escherichia coli*, *Pseudomonas aeruginosa*) bacteria suggesting strong and promising action against the biological system.

Materials and methods

Synthesis of $NiCo_2S_4$ nanostructures

In a typical synthesis, 40 ml of double-distilled water was used to dissolve 0.2 M of the Nickel (II) acetate tetrahydrate and 0.4 M and cobalt (II) acetate tetrahydrate. The mixture was agitated at 450 rpm for 30 min. The mixed solution was placed in a Teflon-lined stainless-steel autoclave and heated to 180 °C for 5 h. The black solution was then removed from the autoclave after cooling to room temperature. The solution was then centrifuged numerous times with ethanol and double-distilled (DD) water to remove any remaining contaminants. Subsequently, the dark colloidal substances were dried for 24 h at 60 °C. The dry powder was then annealed at 200 °C and named as NCS.

$$\mathrm{Ni(CH_3CO_2)_{24}H_2O} + \mathrm{Co(CH_3CO_2)_{24}H_2O} + \mathrm{CH_4N_2} + \mathrm{(CH_2OH)_2\Delta} \rightarrow \mathrm{NiCo_2S_4}. \quad (1)$$

Characterization techniques

X-ray diffraction analysis was performed using a Bruker advanced X-ray diffractometer (XRD). FTIR spectrometer (PERKIN ELMER was used to record the FTIR spectra. A ZEISS device called EVO-18 was used for scanning electron microscopy (SEM).

Measurement of photocatalytic activity

The degradation of amaranth was used to assess the photocatalytic activity of the $NiCo_2S_4$ when solar light radiation served as the source of light. A quartz photoreactor with a cylindrical jacket was used for the photocatalytic reaction. To ensure the appropriate irradiation, visible light was created using natural sunlight. Water was constantly pumped into the cooling jacket of the photoreactor to maintain the reaction temperature at 25 °C. Subsequently, 300 ml of amaranth (10 µm) was mixed with 0.1 g. To ensure the adsorption–desorption equilibrium at predefined time intervals, the amaranth solution containing a photocatalyst ($NiCo_2S_4$) was magnetically agitated for 30 min in the dark before solar light irradiation. 5 ml sample aliquots were collected every 15 min. To track the changes in the adsorption band in the amaranth UV–visible spectrum, the filtrate was examined using a JASCO UV–Vis spectrometer-530.

$$\text{The percentage of photodegradation (\%)} = \frac{C_o - C}{C_o}, \quad (2)$$

where C_o is the initial concentration of Amaranth before irradiation (dark) time and C is the final concentration of Amaranth after a certain irradiation time.

Antibacterial activity

The antibacterial activity of the $NiCo_2S_4$ (NCS) nanostructure was evaluated against *Staph Aureus, Bacillus Subtilis* (Gram-positive bacteria), *E. Coli,* and *Pseudomonas aeruginosa* (gram-negative bacteria). The Kirby-Bauer agar disk diffusion method was used, in which the plates had initially thoroughly dried, and measuring the pH of the medium at the time of preparation and needed to be between 7.2 and 7.4. The tubes containing the bacterial suspensions were kept at 35–37 °C for 2 h. A sterile cotton swab was used to wipe the pathogens onto agar plates after adjusting the suspension to a McFarland standard of 0.5. The inhibition zones were estimated using the common medication amikacin after the plates had been dried and incubated at 37 °C for 18 h.

Result and discussion

Physico-chemical properties

The XRD pattern of the $NiCo_2S_4$ nanostructure is shown in Fig. 1a. The diffracted peaks at 2θ values of 29.8°, 31.5°, 39.8°, 40.2°, 48.6°, 55.0°, and 60.3° are corresponding to Miller indices (281), (311), (398), (418), (493), (515), and (568), respectively, confirming the formation of the cubic crystal structure of the $NiCo_2S_4$ nanomaterials. These peaks

are in good agreement with JCPDS Data 20–0782. XRD pattern of NCS exhibited pure phase formation of $NiCo_2S_4$ nanostructure.

The molecular structure and presence of various functional groups in the NCS nanostructures were identified using the FTIR spectra shown in Fig. 1b. The sharp peak at 620 cm^{-1} corresponds to the Ni/Co-S bending vibrations of the $NiCo_2S_4$ nanostructures. In addition to that, the vibration peak at 893 cm^{-1} reveals the Co-S tensile vibrational mode of the nanoparticle. The stretching vibrations at 1537 cm^{-1}, 1659 cm^{-1}, and the broadband at 3926 cm^{-1} correspond to the O–H stretching vibrational mode of the $NiCo_2S_4$ nanostructures. The morphological variation in the $NiCo_2S_4$ (NCS) nanostructure was recorded using SEM images, as shown in Fig. 1c and d. During the growth process of the nanoparticles, the reaction mechanism was controlled by thiourea. Herein, thiourea acted as a reacting agent and controlled the uniform morphology and agglomeration-less formation of nanoparticles.

Photocatalytic activity

The photocatalytic activity of the $NiCo_2S_4$ nanostructures was evaluated by the degradation of 10 µm Amaranth dye. The changes in the absorption of amaranth dye as a function of irradiation time using $NiCo_2S_4$ nanostructures (0.1 g L^{-1}) are shown in Fig. 2a. The sharp absorption peak of the amaranth dye was shifted to 467 nm by adding 0.1 g L^{-1} of $NiCo_2S_4$ nanostructures under solar radiation with a time interval of 0–20 min. When the sample is irradiated

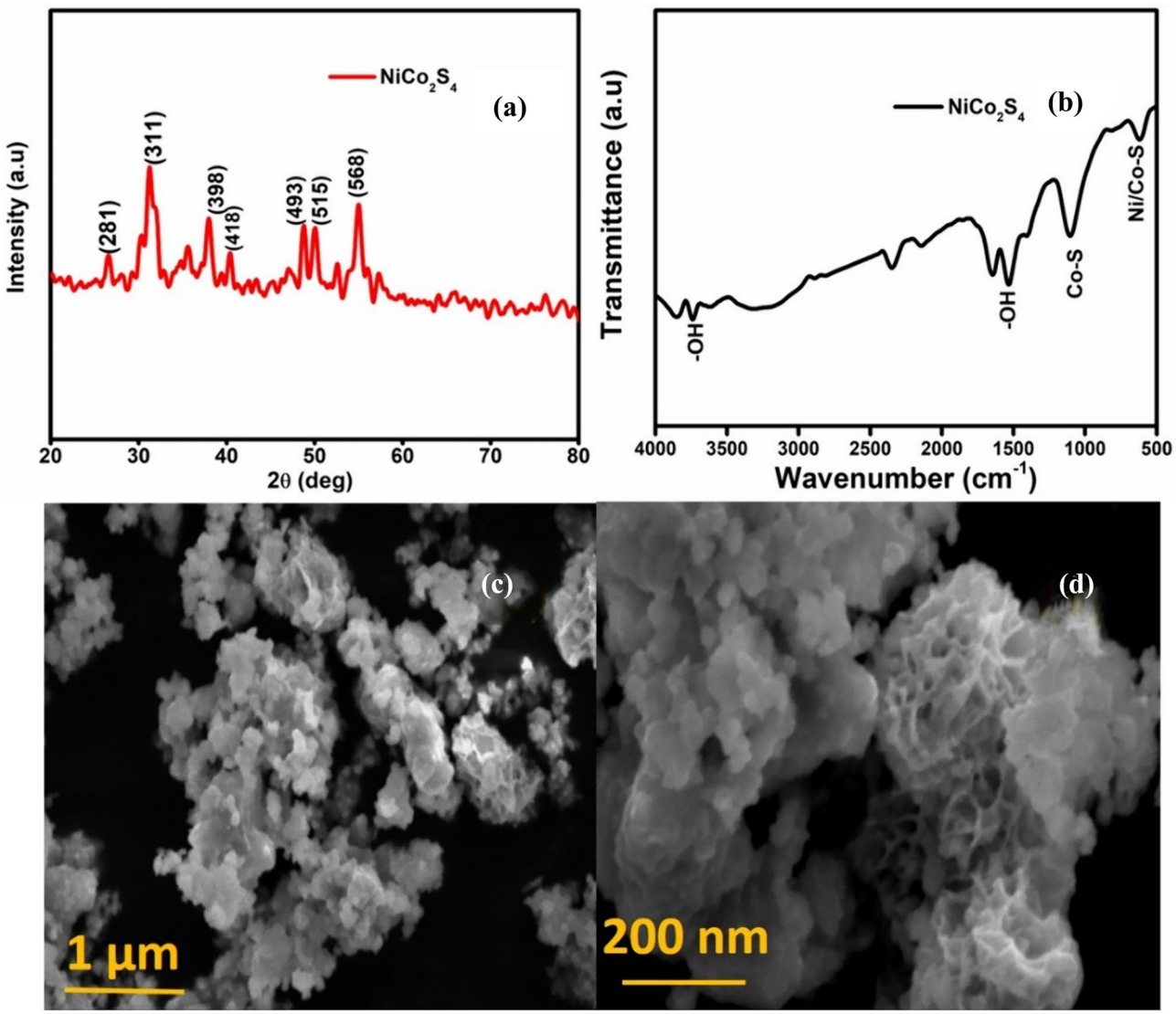

Fig. 1 **a** Powder XRD pattern, **b** FTIR spectrum, and **c**, **d** SEM images of $NiCo_2S_4$ nanostructure

with solar radiation, the amaranth dye has efficiently degraded, as confirmed by the decreasing peak intensity. By increasing the solar radiation time interval from 0 to 120 min, a peak shift was observed and the intensity of the peak decreased gradually. The lowest absorbance peak of the amaranth solution with $NiCo_2S_4$ nanostructures as the catalyst was obtained by 120 min after the irradiation with solar light. This confirms the degradation of the dye material. The higher efficiency of dye degradation is due to the narrow bandgap of the $NiCo_2S_4$ nanostructures (2.14 nm), which facilitates electron transmission from the catalyst to oxygen (O_2) under solar radiation. Thus, the formation of oxygen radicals resulted in strong oxidizing agents that degraded the dye into oxides and water molecules, as mentioned in the reaction.

Figure 2a shows the plot between the wavelength and intensity for the effect of solar light irradiation. Figure 2b shows the variation of absorbance ratio (A/A_o) vs irradiation time. Figure 2c. shows the ln (A/A_o) vs time in min. Figure 2d shows the percentage efficiency of the degradation of amaranth dye. At 120 min, no peak was observed, indicating a 93% degradation efficiency of the $NiCo_2S_4$ nanostructures. The superior degradation efficiency indicates that the $NiCo_2S_4$ nanostructures act as potential catalysts to completely degrade the amaranth dye within 120 min. Therefore, the $NiCo_2S_4$ nanostructures exhibit collegial effects, which are valuable for intractable organic degradation.

The reaction mechanism of the catalyst material with the dye under solar radiation is explained as follows:

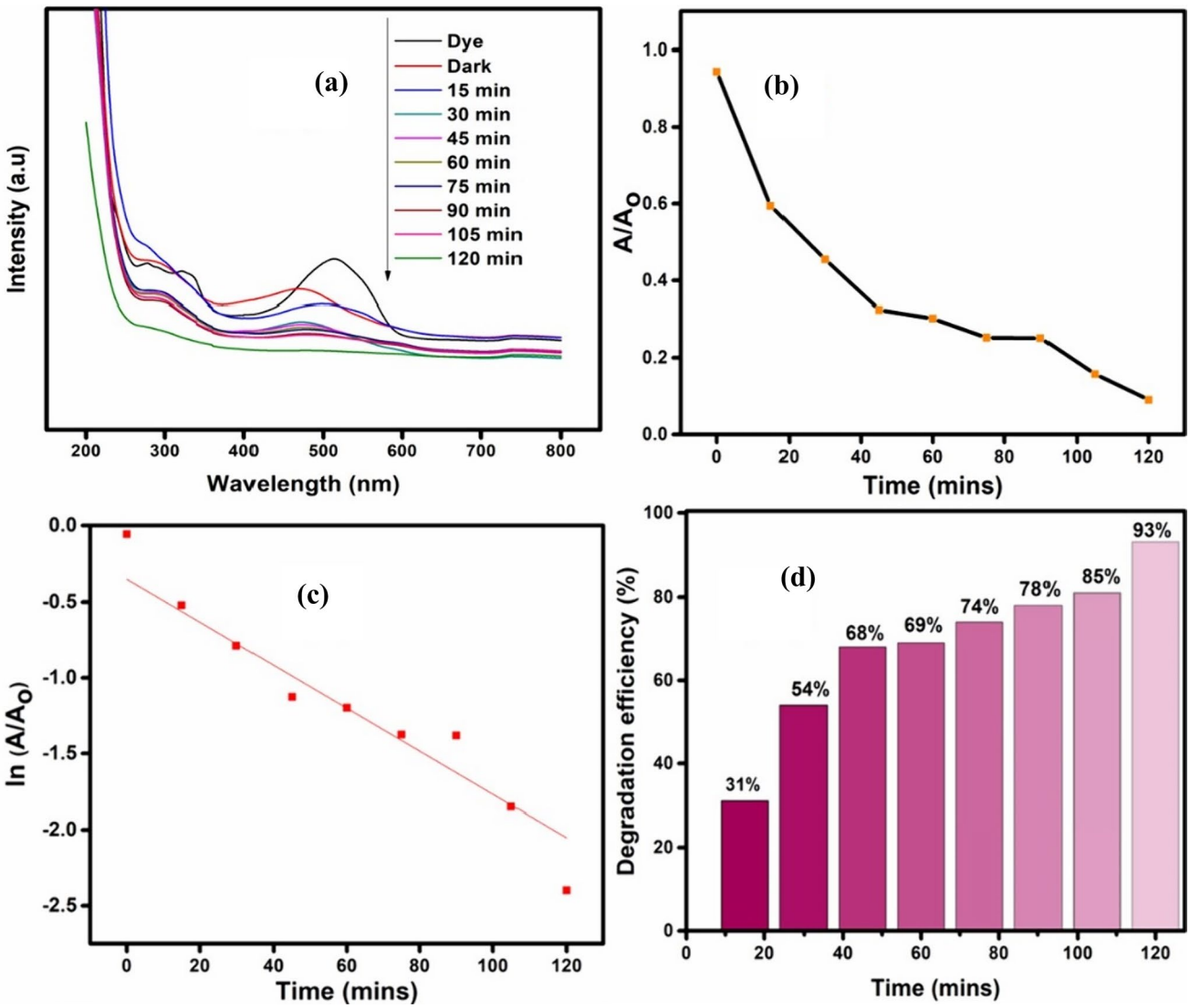

Fig. 2 **a** Absorption changes of Amaranth photodegradation under solar radiation using $NiCo_2S_4$, **b** (A/A_o) ratio, **c** ln (A/A_o) ratio, **d** degradation efficiency

$$NiCo_2S_4 + h\nu \rightarrow e^- + h^+ \quad (3)$$

$$h^+ + H_2O \rightarrow OH^{\cdot} + H^+, \quad (4)$$

$$e^- + O_2 \rightarrow O_2^{\cdot -}, \quad (5)$$

$$O_2^{\cdot} + AN \rightarrow AN^{+\cdot -} O_2, \quad (6)$$

$$OH^{\cdot} + AN^{+\cdot} \rightarrow CO_2 + H_2O + SO_3 \quad (7)$$

Improved photocatalytic detoxification (conversion of organic molecules to inorganic compounds) employing $NiCo_2S_4$ nanostructures is explained in detail in Fig. 3. The electrons (e^-) from the valence band are stimulated to the conduction band for solar radiation. A similar number of holes (h^+) were present in the valence band following the transition of the electron from the valence band to the conduction band. Photogeneration has occurred in the composite material at that precise moment. Oxygen (O_2) attracts electrons to create oxygen radicals ($O_2^{\cdot}$), and water molecules fill the holes to create hydroxyl radicals ($OH^{\cdot}$). The breakdown of organic contaminants into inorganic molecules is caused by oxygen and hydroxyl radicals [2, 11–14].

Antibacterial activities

The antibacterial activity of the synthesized $NiCo_2S_4$ nanostructures was investigated against selected pathogens, such as *Escherichia Coli*, *Pseudomonas aeruginosa*, *Staphylococcus aureus*, and *Bacillus Subtilis*, using the disk diffusion method, and the results are shown in Fig. 4 and Table 1. The synthesized $NiCo_2S_4$ exhibited strong antibacterial activity against both bacterial strains. This indicated that $NiCo_2S_4$ nanostructures showed a high inhibition zone area against all bacterial strains. This may be due to the small crystalline size and the unique sheet-like morphology of the material. Modification of the inhibitory zone reveals the susceptibility of the material to both Gram-positive and Gram-negative bacteria. This can be explained by variations in the morphological composition of these bacteria. Gram-negative bacteria have an outer lipopolysaccharide (LPS) membrane that prevents antibacterial chemicals from passing through the cell wall. The outer peptidoglycan layer alone is not a sufficient permeability barrier, and gram-positive bacteria are more vulnerable to this [15–17]. Gram-negative bacteria have more complex cell walls than gram-positive bacteria. They also serve as the diffusion barriers, which reduce their susceptibility to antibacterial agents. One of the primary propositions of antibacterial methods is the release of S^{2-} from $NiCo_2S_4$, which impedes bacterial cell activities, including

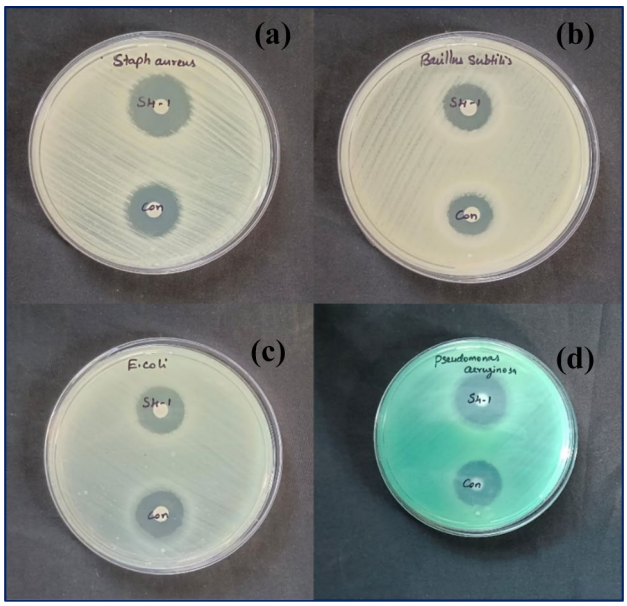

Fig. 4 Antibacterial activity of $NiCo_2S_4$ nanoparticles (**a**, **b**) Gram-positive bacteria (**c**, **d**) Gram-negative bacteria

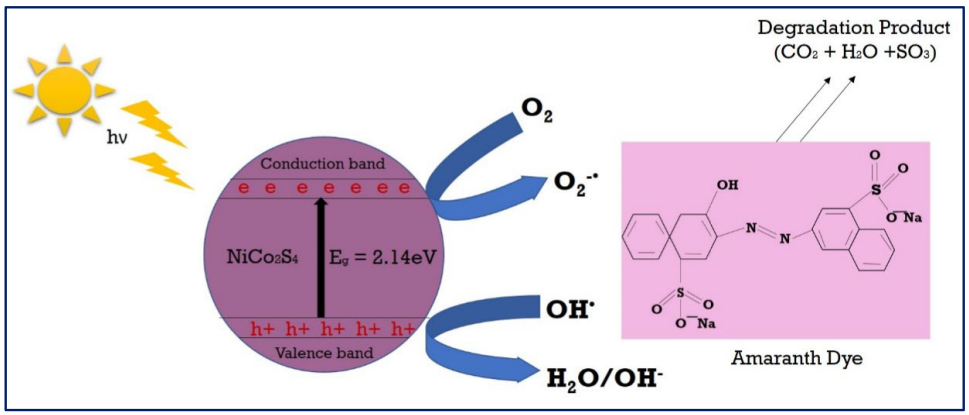

Fig. 3 Schematic diagram of the photocatalytic mechanism

Table 1 Area of inhibition zone (mm) of $NiCo_2S_4$ nanoparticles against Gram-Positive and Gram-negative bacterial Strains

Bacterial strains	Inhibition (mm)	Control (Amikacin) (mm)
Staph aureus	24	20
Bacillus subtilis	18	15
E. coli	20	18
Pseudomonas aeruginosa	24	21

enzyme activity and metabolism, and ultimately causes bacterial cell death. In another way, the $NiCo_2S_4$ nanomaterial attaches to the bacterial cell membrane, causing bacterial cell death.

Conclusion

The $NiCo_2S_4$ nanostructures were successfully synthesized by a hydrothermal method. The powder XRD pattern confirms the formation of a cubic crystal structure of the $NiCo_2S_4$ nanostructures. $NiCo_2S_4$ nanostructures are highly effective as solar-light-active photocatalysts for the degradation of amaranth. The highest photocatalytic activity was attributed mainly to the minimized crystal size and small band gap. 93% of degrading efficiency was observed after 120 min of the degradation process. The synthesized $NiCo_2S_4$ nanostructures have also proved to be an effective antibacterial agent against both Gram-positive (*Staph aureus*, *Bacillus subtilis*) and Gram-negative (*Escherichia coli*, *Pseudomonas aeruginosa*) bacteria suggesting strong and promising action against the biological system.

Acknowledgments The authors are grateful to Jayaraj Annapackiam College for Women (Autonomous), Periyakulam, Tamil Nadu, India for providing financial support through the JACFRP project scheme

Author contributions ABS: conceptualization, methodology, validation, formal analysis, data curation, writing—original draft, and writing—review and editing. RMM, AJCM, AJC, and SS; methodology, validation, formal analysis, software, data curation, resources, and writing—original draft. All authors are approving the final version of the manuscript to be published.

Funding Not applicable.

Data availability The datasets used and/or analyzed during the current study are available from the corresponding author upon reasonable request.

Declarations

Competing interests All authors declare that there are no competing interests.

Ethical approval Not applicable.

References

1. A. Subalakshmi, B. Kavitha, A. Karthika, S. Nikhil, N. Srinivasan, M. Rajarajan, A. Suganthi, Design of Mn and Zr incorporated Ag_2O nanoparticles and their enhanced photocatalytic activity driven by visible light irradiation for degradation of rose bengal dye. New J. Chem. **45**, 1876–1886 (2021)
2. G.M. Zuo, Z.X. Cheng, H. Chen, G.W. Li, T. Miao, Study on photocatalytic degradation of several volatile organic compounds. J. Hazard. Mater. **128**, 158–163 (2006)
3. A. Di Paola, V. Augugliaro, L. Palmisano, G. Pantaleo, E. Savinov, Heterogeneous photocatalytic degradation of nitrophenols. J. Photochem. Photobiol. **155**, 207–214 (2003)
4. H. Karimi-Maleh, B.G. Kumar, S. Rajendran, J. Qin, S. Vadivel, D. Durgalakshmi, F. Gracia, M. Soto-Moscoso, Y. Orooji, F. Karimi, Tuning of metal oxides photocatalytic performance using Ag nanoparticles integration. J. Mol. Liq. **314**, 113588 (2020)
5. M.C. Roşu, C. Socaci, V. Floare-Avram, G. Borodi, F. Pogăcean, M. Coroş, L. Măgeruşan, S. Pruneanu, Photocatalytic performance of graphene/TiO_2-Ag composites on amaranth dye degradation. Mater. Chem. Phys. **179**, 232–241 (2016)
6. M.S. Amulya, H.P. Nagaswarupa, M.A. Kumar, C.R. Ravikumar, K.B. Kusuma, Sonochemical synthesis of $MnFe_2O_4$ nanoparticles and their electrochemical and photocatalytic properties. J. Phys. Chem. Solids **148**, 109661 (2021)
7. E. Jiang, N. Song, G. Che, C. Liu, H. Dong, L. Yang, Construction of a Z-scheme MoS_2/$CaTiO_3$ heterostructure by the morphology-controlled strategy towards enhancing photocatalytic activity. Chem. Eng. J. **399**, 125721 (2020)
8. J. Yang, C. Bao, K. Zhu, T. Yu, F. Li, J. Liu, Z. Li, Z. Zou, High catalytic activity and stability of nickel sulfide and cobalt sulfide hierarchical nanospheres on the counter electrodes for dye-sensitized solar cells. Chem. Commun. **50**, 4824–4826 (2014)
9. S.M. Reda, Synthesis of ZnO and Fe_2O_3 nanoparticles by sol–gel method and their application in dye-sensitized solar cells. Mater. Sci. Semicond. Process. **13**, 417–425 (2010)
10. R.S. Dubey, S.R. Jadkar, A.B. Bhorde, Synthesis and characterization of various doped TiO_2 nanocrystals for dye-sensitized solar cells. ACS Omega **6**, 3470–3482 (2021)
11. S. Chandran, R. Paulraj, P. Ramasamy, Influence of amaranth dye on the growth and properties of KDP single crystal. Mater. Res. Bull. **68**, 210–215 (2015)
12. J.R. Steter, W.R. Barros, M.R. Lanza, A.J. Motheo, Electrochemical and sonoelectrochemical processes applied to amaranth dye degradation. Chemosphere **117**, 200–207 (2014)
13. A. Bassi, K. Qanungo, I. Hasan, A.A. Alshayiqi, A.S. Ababtain, F.A. Alharthi, CuO nanorods immobilized agar-alginate biopolymer: a green functional material for photocatalytic degradation of amaranth dye. Polymers **15**, 553 (2023)
14. S.M.F. Khyrun, A.J. Christy, J. Mayandi, S. Sagadevan, Photo-triggered antibacterial and catalytic activities of solution combustion synthesized CeO_2/NiO binary nanocomposite. Inorg. Chem. Commun **153**, 110860 (2023)

15. A.A. Menazea, A.M. Ismail, N.S. Awwad, H.A. Ibrahium, Physical characterization and antibacterial activity of PVA/Chitosan matrix doped by selenium nanoparticles prepared via one-pot laser ablation route. J. Mater. Res. Technol. **9**, 9598–9606 (2020)
16. K. Gurning, H.A. Simanjuntak, H. Purba, R.F. Situmorang, L. Barus, S. Silaban, Determination of total tannins and antibacterial activities ethanol extraction seri (*Muntingia calabura* L.) leaves. J. Phys. **811**, 012121 (2021)
17. M.G. Demissie, F.K. Sabir, G.D. Edossa, B.A. Gonfa, Synthesis of zinc oxide nanoparticles using leaf extract of Lippia Adoensis (koseret) and evaluation of its antibacterial activity. J. Chem. **2020**, 1–9 (2020)